Chinese Chemical Letters 33 (2022) 1110–1115

Contents lists available at ScienceDirect

Chinese Chemical Letters

journal homepage: www.elsevier.com/locate/cclet

New electron-donating segment to develop thermally activated delayed fluorescence emitters for efficient solution-processed non-doped organic light-emitting diodes

Ming Zhang[a,b], Gaole Dai[b], Caijun Zheng[a,*], Kai Wang[b], Yizhong Shi[b], Xiaochun Fan[b], Hui Lin[a], Silu Tao[a], Xiaohong Zhang[b,*]

[a] School of Optoelectronic Science and Engineering, University of Electronic Science and Technology of China (UESTC), Chengdu 610054, China
[b] Institute of Functional Nano & Soft Materials (FUNSOM), Soochow University, Suzhou 215123, China

ARTICLE INFO

Article history:
Received 5 July 2021
Revised 30 July 2021
Accepted 12 August 2021
Available online 18 August 2021

Keywords:
Electron-donating segment
Thermally activated delayed fluorescence
Solution process
Non-doped emitter
Organic light-emitting diode

ABSTRACT

Thermally activated delayed fluorescent (TADF) materials capable of efficient solution-processed non-doped organic light-emitting diodes (OLEDs) are of important and practical significance for further development of OLEDs. In this work, a new electron-donating segment, 2,7-di(9*H*-carbazol-9-yl)-9,9-dimethyl-9,10-dihydroacridine (2Cz-DMAC), was designed to develop solution-processable non-doped TADF emitters. 2Cz-DMAC can not only simultaneously increase the solubility of compounds and suppress harmful aggregation-caused quenching, but also efficiently broaden the delocalization of the highest occupied molecular orbital and promote the reverse intersystem crossing process. Three new TADF emitters, 2-(2,7-di(9*H*-carbazol-9-yl)-9,9-dimethylacridin-10(9*H*)-yl)dibenzo[b,d]thiophene 5,5-dioxide (2Cz-DMAC-BTB), 2-(2,7-di(9*H*-carbazol-9-yl)-9,9-dimethylacridin-10(9*H*)-yl)-9H-thioxanthen-9-one (2Cz-DMAC-TXO), 2-(2,7-di(9*H*-carbazol-9-yl)-9,9-dimethylacridin-10(9*H*)-yl)thianthrene 5,5,10,10-tetraoxide (2Cz-DMAC-TTR), were developed by using 2Cz-DMAC segment as the electron-donor. As anticipated, the solution-processed non-doped OLEDs employing 2Cz-DMAC-BTB, 2Cz-DMAC-TXO and 2Cz-DMAC-TTR as the emitters respectively exhibited green, orange and red emissions with maximum external quantum efficiencies of 14.0%, 6.6% and 2.9%. These results successfully demonstrate the feasibility and convenience of developing efficient solution-processable non-doped TADF emitters based on 2Cz-DMAC segment.

Thermally activated delayed fluorescent (TADF) materials with the merit of harvesting both singlet and triplet excitons for theoretically 100% internal quantum efficiency have been attracted special attention in recent years owing to their great potential applications in organic light-emitting diodes (OLEDs) [1,2]. Till now, highly efficient OLEDs based on TADF emitters in all colors have successfully surpassed 30% external quantum efficiencies (EQEs), which are obviously comparable with the best phosphorescent OLEDs [3-9]. Nevertheless, for most TADF-OLEDs, the emitting layers (EML) are optimized with a host-dopant configuration [1,10-13]. And such multicomponent EML would not only require precise control on doping ratios and high cost of fabrication, but also induce fatal phase separation during operation [14,15]. Obviously, non-doped EML possessing only emitter itself is more attractive for mass production [14,16-18]. Meanwhile, solution process is more attractive for industry manufacture because of its unique advantages, such as simple device structures, easy and low-cost device fabrications and the feasibility for flexible devices [19-22]. Therefore, TADF emitters capable of efficient solution-processed non-doped OLEDs are of practical and important significance for the further development of OLEDs.

As an idea solution-processable non-doped TADF emitter, some requirements should be met (i) favorable solubility, good thermal and morphological stability *via* solution processing; (ii) effectively restraining concentration aggregation-caused quenching (ACQ) to avoid energy loss; (iii) efficient TADF to realize full exciton utilization [7,17,20,23-26]. Although polymers and dendrimers have the potential to fulfill these requirements, the macromolecules are hard to be synthesized and purified, restraining their performance and development [12,21,23,27-30]. Reversely, small-molecule compounds have the superiorities on synthesis and purification, and are also more flexible on design. Accordingly, small-molecule TADF

* Corresponding authors.
E-mail addresses: zhengcaijun@uestc.edu.cn (C. Zheng), xiaohong_zhang@suda.edu.cn (X. Zhang).

https://doi.org/10.1016/j.cclet.2021.08.064
1001-8417/

emitters are regarded as the ideal candidates to develop solution-processed non-doped OLEDs [4,15,17,31-34]. To develop solution-processable non-doped small-molecule emitters, the general strategy is encapsulating evaporation-processed emitters with alkyl chains, which could increase their solubility as well as decrease harmful ACQ process by preventing the intermolecular interaction [21,35,36]. However, these external alkyl chains always seriously reduce the molecular rigidity, and the resulting enhanced molecular relaxation harms the exciton utilizations of the emitters [37-41]. Therefore, a feasible and promising approach to develop solution-processable non-doped TADF emitter without alkyl chains is essential and important [16,24,26,31,32,42-44].

In this work, we designed a new electron-donating segment, 2,7-di(9*H*-carbazol-9-yl)-9,9-dimethyl-9,10-dihydroacridine (2Cz-DMAC), in which, two carbazole (Cz) groups are attached at the C2 and C7 position of 9,9-dimethyl-9,10-dihydroacridine (DMAC). In this segment, conjugation can be happened between Cz and DMAC groups, which will efficiently broaden the delocalization of the highest occupied molecular orbital (HOMO), promoting the reverse intersystem crossing (RISC) process to enhance TADF [2]. Meanwhile, as the similar-structure multi-carbazole segment was widely reported to develop dendrimers, 2Cz-DMAC might also increase the solubility of molecules. Besides, the large steric hindrance of two attached Cz groups could also prevent the intermolecular interaction, effectively suppressing harmful ACQ. Therefore, 2Cz-DMAC-based compounds have the potential to meet above three requirements to act as the solution-processable non-doped TADF emitters. Accordingly, we developed three new TADF emitters, namely 2-(2,7-di(9*H*-carbazol-9-yl)-9,9-dimethylacridin-10(9*H*)yl)dibenzo[b,d]thiophene 5,5-dioxide (2Cz-DMAC-BTB), 2-(2,7-di(9*H*-carbazol-9-yl)-9,9-dimethylacridin-10(9*H*)-yl)-9H-thioxanthen-9-one (2Cz-DMAC-TXO) and 2-(2,7-di(9*H*-carbazol-9-yl)-9,9-dimethylacridin-10(9*H*)-yl)thianthrene 5,5,10,10-tetraoxide (2Cz-DMAC-TTR), by combining 2Cz-DMAC with different electron-accepting groups of dibenzo[b,d]thiophene 5,5-dioxide (BTB), 9*H*-thioxanthen-9-one (TXO) and thianthrene 5,5,10,10-tetraoxide (TTR). As anticipated, 2Cz-DMAC-BTB, 2Cz-DMAC-TXO and 2Cz-DMAC-TTR exhibited good solubility, thermal stability and film-forming ability as well as evident TADF characteristics with extremely small energy gaps between S_1 and T_1 states (ΔE_{ST}s) of 0.020, 0.036 and 0.047 eV, respectively. In solution-processed neat films, 2Cz-DMAC-BTB, 2Cz-DMAC-TXO and 2Cz-DMAC-TTR exhibited high photoluminescence quantum yields (Φ_{PL}s) of 68.0%, 32.2% and 12.6%, and high rate constants of RISC process (k_{RISC}) of 12.6 × 10^5, 8.6 × 10^5 and 5.7 × 10^5 s^{-1}, respectively. By employing 2Cz-DMAC-BTB, 2Cz-DMAC-TXO and 2Cz-DMAC-TTR as the emitters, the optimized solution-processed non-doped OLEDs realized maximum EQEs of 14.0%, 6.6% and 2.9% with green, orange and red emission, respectively. These results demonstrated 2Cz-DMAC was an ideal electron-donating segment to develop efficient solution-processable non-doped TADF emitters.

All reagents were purchased from commercial sources and used as received without further purification. Solvents for synthesis were purified according to standard procedures prior to use. The synthetic routes towards 2Cz-DMAC-BTB, 2Cz-DMAC-TXO and 2Cz-DMAC-TTR are shown in Scheme 1. The detailed synthesis procedure of 2Cz-DMAC segment was described in the Experimental Section. And 2Cz-DMAC-BTB, 2Cz-DMAC-TXO and 2Cz-DMAC-TTR were finally synthesized from the $Pd(OAc)_2$ catalyzed cross-coupling reaction between dibenzo[*b*,*d*]thiophene 5,5-dioxide (BTB), 9H-thioxanthen-9-one (TXO), thianthrene 5,5,10,10-tetraoxide (TTR) and 2Cz-DMAC. The chemical structures of the intermediates and target compounds were fully characterized and confirmed by nuclear magnetic resonance (NMR) spectroscopy and mass spectrometry (MS). Before characterization, 2Cz-DMAC-BTB, 2Cz-DMAC-TXO and 2Cz-DMAC-TTR were further purified by sublimation.

The thermal properties of three compounds were measured by differential scanning calorimetry (DSC) and thermogravimetric analysis (TGA) under nitrogen atmosphere. As shown in Fig. S15 (Supporting information) and Table 1, the decomposition temperatures (T_d, corresponding to 5% weight loss) of 2Cz-DMAC-BTB, 2Cz-DMAC-TXO and 2Cz-DMAC-TTR are as high as 448, 444 and 436 °C. Meanwhile, no phase transition, like the melting and the glass transition, was observed during the tested temperature range in the DSC measurement, indicating the amorphous characteristic of three compounds.

To investigate the solubility of 2Cz-DMAC-based compounds. a simple 2Cz-DMAC derivative 2,7-di(9*H*-carbazol-9-yl)-9,9-dimethyl-10-phenyl-9,10-dihydroacridine (2Cz-DMAC-Ph) was also synthesized. And 2Cz-DMAC-Ph exhibited a high solubility of >84.0 mg/mL by dissolved in chlorobenzene solution, suggesting satisfactory solubility of 2Cz-DMAC segment. As listed in Table S2 (Supporting information), the solubilities of 2Cz-DMAC-BTB, 2Cz-DMAC-TXO and 2Cz-DMAC-TTR in chlorobenzene solution respectively are ~66.0, >22.0 and ~11.0 mg/mL, indicating they can be treated *via* the solution process. Then, the atomic force microscopy (AFM) 3D images were investigated since the surface topography of the film could have great influence on the performance of solution-processed OLEDs. As shown in Fig. 1, we measured the morphologies of spin-coated neat films of three compounds on the silicon substrate. The root-mean-square (RMS) surface roughness values were 0.240, 0.312 and 0.266 nm for 2Cz-DMAC-BTB, 2Cz-DMAC-TXO and 2Cz-DMAC-TTR neat films, respectively. These results confirm that three 2Cz-DMAC-based compounds can be used to construct solution processed OLEDs.

The frontier molecular orbital distributions of three compounds were analyzed with density function theory (DFT) calculations on the ground state at the B3LYP/6-31G(d) level. As shown in Fig. 2, the lowest unoccupied molecular orbitals (LUMOs) of 2Cz-DMAC-BTB, 2Cz-DMAC-TXO and 2Cz-DMAC-TTR are confined on the BTB, TXO and TTR moieties, respectively; while their HOMOs are widely spread over whole 2Cz-DMAC segment, indicating the effective delocalization of HOMO distributions caused by strong conjugation between Cz and DMAC groups. All three compounds display evident separations between the HOMOs and LUMOs, which will benefit them to realize extremely small ΔE_{ST}s with the predicted values of 0.012, 0.015 and 0.009 eV for 2Cz-DMAC-BTB, 2Cz-DMAC-TXO and 2Cz-DMAC-TTR, respectively. Thus, three compounds would have effective RISC process and consequently evident TADF characteristic. Meanwhile, the calculated oscillator strength (*f*) values of 2Cz-DMAC-BTB, 2Cz-DMAC-TXO and 2Cz-DMAC-TTR were estimated to be 0.0010, 0.0012 and 0.0008, consistent with the slight overlap between the HOMO and LUMOs.

The electrochemical properties of 2Cz-DMAC-BTB, 2Cz-DMAC-TXO and 2Cz-DMAC-TTR were subsequently measured by the cyclic voltammetry (CV) measurement. As depicted in Fig. S16 (Supporting information), determined from the onsets of the oxidation curves with respect to that of ferrocene, the HOMO energy levels of three compounds showed almost close values of 5.53, 5.56 and 5.59 eV, respectively, which would be mainly ascribed to the identical electron-donating segment 2Cz-DMAC. Meanwhile, the LUMO energy levels were calculated to be -3.07, -3.28 and -3.46 eV from the onsets of the reduction curves for 2Cz-DMAC-BTB, 2Cz-DMAC-TXO and 2Cz-DMAC-TTR. Accordingly, the electrochemical bandgaps of 2Cz-DMAC-BTB, 2Cz-DMAC-TXO and 2Cz-DMAC-TTR were calculated to be 2.46, 2.28 and 2.13 eV, corresponding to green, yellow and orange-red emission.

The photophysical properties of three compounds were then investigated by using ultraviolet-visible (UV-vis) spectrophotometer

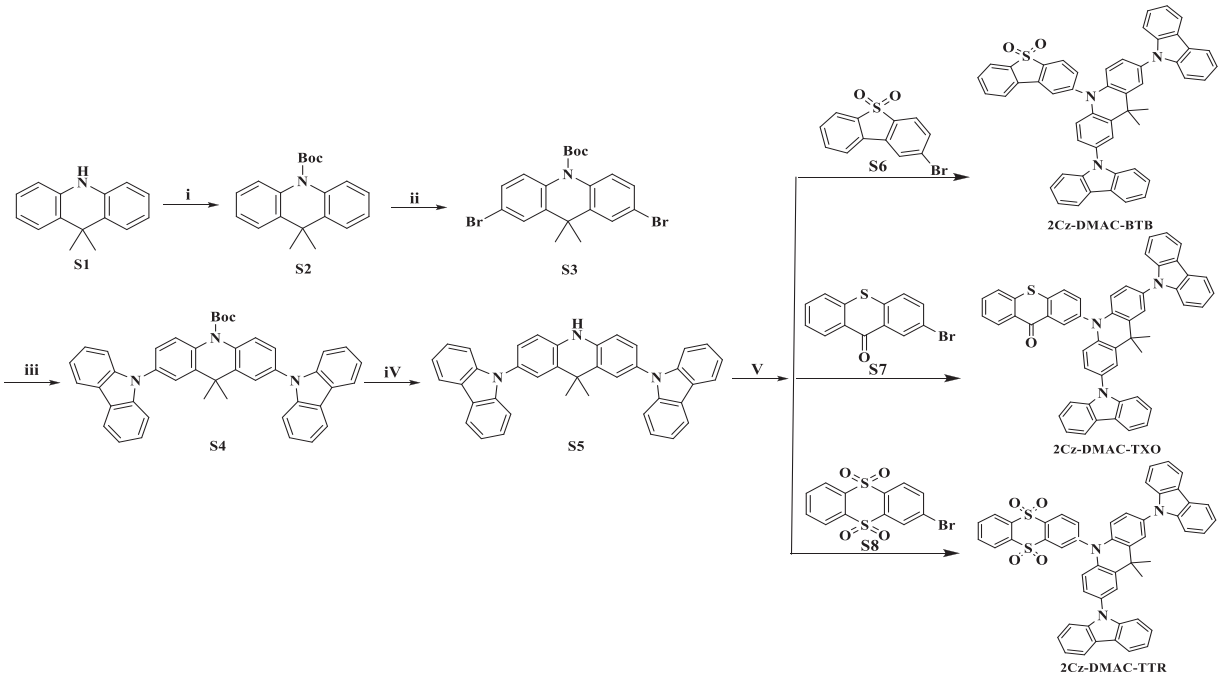

Scheme 1. Synthetic routes and molecular structures of 2Cz-DMAC-BTB, 2Cz-DMAC-TXO and 2Cz-DMAC-TTR. (i) DMAP, $(Boc)_2O$, THF, 0 °C to reflux, 2 h, yields: 96%; (ii) r.t. 5 h, then 80°C, 10 h, NBS, DCM/AcOH, yields: 82%; (iii)$Pd(OAc)_2$, $P(tBu)_3$, ^{t}BuONa, toluene, reflux, 12 h, yields: 72%; (iv) TFA, DCM, r.t. 12 h, yields: 90%; (v) $Pd(OAc)_2$, $P(tBu)_3$, ^{t}BuONa, toluene, reflux, 12h, yields of 74%, 78% and 68% for 2Cz-DMAC-BTB, 2Cz-DMAC-TXO and 2Cz-DMAC-TTR, respectively.

Table 1
Thermal, photophysical and electrochemical properties of 2Cz-DMAC-BTB, 2Cz-DMAC-TXO and 2Cz-DMAC-TTR.

Compounds	λ_{abs}[a] (nm)	λ_{PL}[a] (nm)	HOMO[b] (eV)	LUMO[c] (eV)	E_g[d] (eV)	S_1/T_1[e] (eV)	ΔE_{ST}[f] (eV)	Φ_{PL}[g] (%)	f[h]	T_d[i] (°C)	k_{RISC}[j] ($\times 10^5$ s^{-1})	k_{nr}[Tk] ($\times 10^5$ s^{-1})
2Cz-DMAC-BTB	313/400	510	-5.53	-3.07	2.46	2.463/2.443	0.020	68.0	0.0010	448	12.6	1.50
2Cz-DMAC-TXO	316/425	560	-5.56	-3.28	2.28	2.311/2.275	0.036	32.2	0.0012	444	8.6	4.06
2Cz-DMAC-TTR	316/452	594	-5.59	-3.46	2.13	2.238/2.191	0.047	12.6	0.0008	436	5.7	12.5

[a] Measured in toluene at room temperature;
[b] Measured HOMO energy level;
[c] Measured LUMO energy level;
[d] The electrochemical bandgap between the HOMO and LUMO energy levels;
[e] Determined from the energy peak of the fluorescence and phosphorescence spectra of three compounds neat films at 77 K;
[f] The energy gap between the singlet and triplet state energy;
[g] Φ_{PL} is the total photoluminescence fluorecence quantum efficiency value;
[h] The value of oscillator strength;
[i] Decomposition temperature corresponding to 5% weight loss;
[j] The rate constant of reverse intersystem crossing;
[k] The rate constant of triplet non-radiative transition.

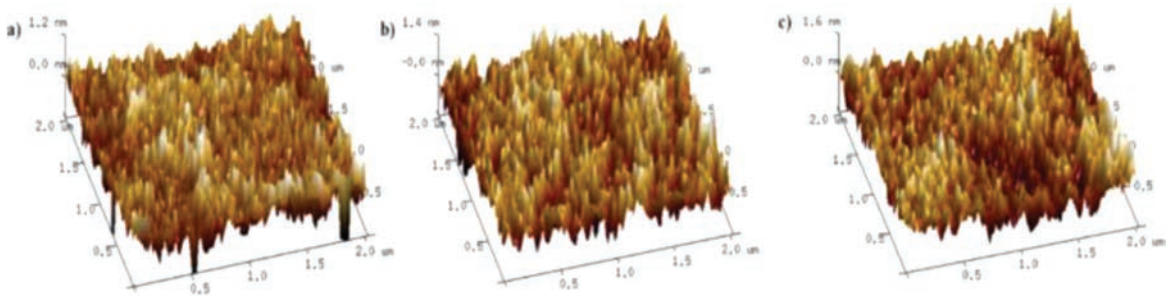

Fig. 1. 3D AFM height images of the solution-processed films (60 nm thickness) on silicon substrate. (a) 2Cz-DMAC-BTB neat film, (b) 2Cz-DMAC-TXO neat film, (c) 2Cz-DMAC-TTR neat film.

and PL spectrometers. As presented in Fig. 3a, from the UV absorption spectra of 2Cz-DMAC-BTB, 2Cz-DMAC-TXO and 2Cz-DMAC-TTR in dilute toluene solution at room temperature, two types of absorption bands are observed. The strong absorptions below 320 nm should be mainly attributed to the local excited transition of 2Cz-DMAC, BTB, TXO and TTR moieties. And the broad and weak absorptions at the longer-wavelength region should be attributed to intramolecular charge-transfer transition from 2Cz-DMAC to BTB, TXO and TTR core. Meanwhile, with different electron-drawing abilities (TTR > TXO > BTB), the ICT absorption spectrum of 2Cz-

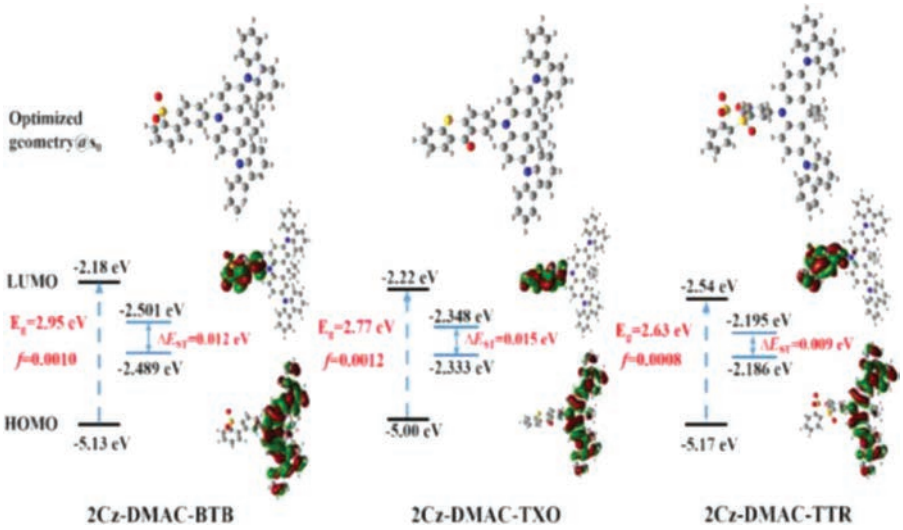

Fig. 2. HOMO and LUMO electronic distributions, energy level, and bandgaps (E_g), the lowest singlet (S_1), and triplet (T_1) and oscillator strengths of S_1 (f) for 2Cz-DAMC-BTB, 2Cz-DMAC-TXO, 2Cz-DMAC-TTR, calculated by DFT at the B3LYP/6-31G* level.

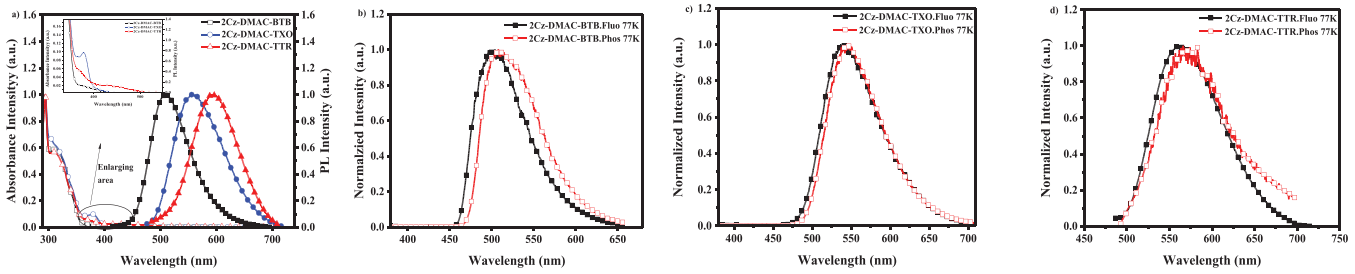

Fig. 3. (a) Absorption and fluorescence spectra of 2Cz-DMAC-BTB, 2Cz-DMAC-TXO and 2Cz-DMAC-TTR in toluene, and refined absorptions of three compounds. (b) Normalized fluorescence and phosphorescence spectra of 2Cz-DMAC-BTB neat film at 77 K. (c) Normalized fluorescence and phosphorescence spectra of 2Cz-DMAC-TXO neat film at 77 K. (d) Normalized fluorescence and phosphorescence spectra of 2Cz-DMAC-TTR neat film at 77 K.

DMAC-TTR was located in a longer wavelength range of 410-494 nm comparing to those of 2Cz-DMAC-TXO (405-455 nm) and 2Cz-DMAC-BTB (367-439 nm). To further prove their ICT characteristic, we further measured the PL spectra of three compounds in different solvents. As shown in Fig. S17 (Supporting information), with solvent polarity gradually increased from non-polar cyclohexane to higher polar toluene and highest polar ethyl acetate, significant solvatochromic effect can be observed for all three compounds. The emission peaks were red-shifted from 494 nm in cyclohexane to 510 nm in toluene with a shift of 26 nm and 553 nm in ethyl acetate with a shift of 59 nm for 2Cz-DMAC-BTB, from 495 nm in cyclohexane to 547nm in toluene with a shift of 52 nm and 589 nm in ethyl acetate with a shift of 94 nm for 2Cz-DMAC-TXO, and from 549 nm in cyclohexane to 591 nm in toluene with a shift of 42 nm and 618 nm in ethyl acetate with a shift of 69 nm for 2Cz-DMAC-TTR. The higher Stokes shift of 2Cz-DMAC-TXO should be ascribed to its higher dipole moment than 2Cz-DMAC-BTB and 2Cz-DMAC-TTR.The aggregation-induced emission (AIE)property of three compounds was also investigated. As shown in Fig. S18 (Supporting information), the PL intensities of three compounds are firstly weakened along with the increasing ratio of water, but then gradually enhanced till the 90%ratio of water. These results indicate three compounds partly show AIE features, which would further suppress ACQ process.

As shown in Fig. 3, Fluorescence and phosphorescence spectra of 2Cz-DMAC-BTB, 2Cz-DMAC-TXO and 2Cz-DMAC-TTR in neat films were measured at 77 K. From the peaks of the fluorescence and phosphorescence spectra, their S_1 and T_1 energy levels are estimated as 2.463 and 2.443 eV for 2Cz-DMAC-BTB, 2.311 and 2.275 eV for 2Cz-DMAC-TXO and 2.238 and 2.191 eV for 2Cz-DMAC-TTR, respectively. And their ΔE_{ST}s are estimated to be 0.020, 0.036, and 0.047 eV for 2Cz-DMAC-BTB, 2Cz-DMAC-TXO and 2Cz-DMAC-TTR. These extremely small ΔE_{ST}s will significantly enhance the RISC process and benefit the utilization of triplet excitons. By using an integrating sphere, the Φ_{PL}s of 2Cz-DMAC-BTB, 2Cz-DMAC-TXO and 2Cz-DMAC-TTR in neat films were measured to be 68.0%, 32.2% and 12.6% under oxygen-free condition. Meanwhile, the transient PL decay curves of three compounds were then investigated**.** At the room temperature, 2Cz-DMAC-BTB, 2Cz-DMAC-TXO and 2Cz-DMAC-TTR neat films showed prompt decays with short lifetimes of 44.4, 47.9 and 22.1 ns in the range of 100 ns and delayed decays with lifetimes of 2.57, 1.93 and 0.76 μs in the range of 10 μs in nitrogen atmosphere. The temperature-dependence transient decay curves of three compounds are shown in Fig. S19. With the temperature increasing from 100 K to 300 K, the delayed lifetime of 2Cz-DMAC-BTB and 2Cz-DMAC-TXO are gradually declined, indicating their TADF characteristics. Relatively, the decay curves of 2Cz-DMAC-TTR are almost independent with the temperatures, which should be ascirbed to the quite weak intensities of its transient decays and unsatisfactory detection limitation of the instrument. To better understand the decay mechanisms of 2Cz-DMAC-BTB, 2Cz-DMAC-TXO and 2Cz-DMAC-TTR, we further analyzed their dynamic excitons variations by calculating their key kinetic parameters. To facilitate the calculations, the internal conversion process of singlet excitons was ignored here as it was evidently weaker compared with fluorescence decay and intersysrem crossing (ISC) process of singlet excitons normally. The key calculations were carried out via

Table 2
The device performance of the solution-processed non-doped OLEDs based on 2Cz-DMAC-BTB, 2Cz-DMAC-TXO and 2Cz-DMAC-DMAC-TTR.

Emitters	V_{on}[a] (V)	λ_{max}[b] (nm)	L_{max}[c] (cd/m^2)	CE/PE/EQE[d](cd/A, lm/W, %)			CIE[e] (x, y)
				Maximum	At 100 cd/m^2	At 1000 cd/m^2	
2Cz-DMAC-BTB	3.3	548	2462	43.3/37.8/14.0	36.9/30.7/11.5	17.4/12.4/5.6	(0.39, 0.54)
2Cz-DMAC-TXO	3.1	572	2555	18.3/17.4/6.6	12.9/10.4/4.7	8.2/5.1/2.9	(0.47, 0.51)
2Cz-DMAC-TTR	3.6	608	550.5	5.0/4.3/2.9	2.8/1.9/1.6	N.A.	(0.56, 0.42)

[a] Turn-on voltage of the device;
[b] EL peak wavelength;
[c] Maximum luminance;
[d] CE: current efficiency, PE: power efficiency, EQE: external quantum efficiency;
[e] Commission Internationale de L'Eclairage coordinate value of the device.

the following equations [2,45]:

$$k_p = \frac{1}{\tau_p} \quad (1)$$

$$k_d = \frac{1}{\tau_d} \quad (2)$$

$$k_F = k_p \Phi_F \quad (3)$$

$$k_{ISC} = k_P(1 - \Phi_F) \quad (4)$$

$$k_{RISC} = \frac{k_p k_d}{k_{ISC}} \frac{\Phi_{TADF}}{\Phi_F} \quad (5)$$

$$k_{nr}^T = k_d - \left(1 - \frac{k_{ISC}}{k_F + k_{ISC}}\right) k_{RISC} \quad (6)$$

where Φ_F and Φ_{TADF} are the quantum efficiencies of prompt and delayed fluorescence; Φ_{ISC} is the efficiency of ISC process; k_p, k_d, k_F, $k_{ISC,}$ k_{RISC} and $k_{nr}{}^T$ are rate constants of prompt fluorescence, delayed fluorescence, fluorescence process from S_1 to S_0 state, ISC process from S_1 to T_1 state, RISC process from T_1 to S_1 state, non-radiative process from T_1 to S_0, respectively. Φ_Fs and Φ_{TADF}s of these emitters were estimated from the Φ_{PL}s with relative ratios which were calculated from the transient PL results. Consequently, we got all key kinetic parameters of 2Cz-DMAC-BTB, 2Cz-DMAC-TXO, 2Cz-DMAC-TTR and listed them in Table S3 (Supporting information). For the RISC process, 2Cz-DMAC-BTB showed an evidently higher k_{RISC} of 12.6 × 10^5 s^{-1} comparing to the 2Cz-DMAC-TXO (8.6 × 10^5 s^{-1}) and the 2Cz-DMAC-TTR (5.7 × 10^5 s^{-1}), which should be mainly attribute to the smallest ΔE_{ST} of 2Cz-DMAC-BTB. Meanwhile, the $k_{nr}{}^T$s of 2Cz-DMAC-BTB, 2Cz-DMAC-TXO and 2Cz-DMAC-TTR were calculated as 1.50 × 10^5, 4.06 × 10^5 and 12.5 × 10^5 s^{-1}, respectively. As the non-radiative process is exponentially inverse correlation with the bandgap of the compound, the $k_{nr}{}^T$ of 2Cz-DMAC-BTB is evidently smaller than those of other two compounds [46,47]. And the small value of 1.50 × 10^5 s^{-1} $k_{nr}{}^T$ should be also derived from 2Cz-DMAC segment suppressing ACQ process in the neat films. Therefore, the evidently different PLQYs of three compounds should be mainly caused by their different energy gaps. With similar oscillator strength values, the k_Fs of three compounds are very close as listed in Table 1 and Table S3. However, the $k_{nr}{}^T$ of 2Cz-DMAC-TTR is significantly higher than those of 2Cz-DMAC-BTB and 2Cz-DMAC-TXO, resulting in a quite poor PLQY.

Finally, the electroluminescence (EL) performance of three solution-processable TADF emitters was evaluated. The solution-processed OLEDs were optimized with a general configuration of ITO/PEDOT:PSS (40 nm)/EMLs (60 nm)/TmPyPB (5 nm)/TPBi (35 nm)/LiF (1 nm)/Al, where 2Cz-DMAC-BTB, 2Cz-DMAC-TXO and 2Cz-DMAC-TTR neat films were served as the EMLs. ITO and LiF/Al act as the anode and the cathode, respectively. TmPyPb (1,3,5-tri(*m*-pyrid-3-yl-phenyl)benzene) and TPBi (1,3,5-tris(*N*-phenylbenzimidazol-2-yl)benzene) were respectively used as the hole-blocking layer (HBL) and electron-transporting layer (ETL). As shown in Fig. 4 and listed in Table 2, three solution-processed OLEDs display low turn-on voltages of 3.3, 3.1 and 3.6 V for 2Cz-DMAC-BTB, 2Cz-DMAC-TXO and 2Cz-DMAC-TTR, respectively. These values are relatively lower than other reported solution-processed non-doped OLEDs, indicating three emitters might have good carrier transporting properties and fluent carrier injection. In the solution-processed OLEDs, 2Cz-DMAC-BTB, 2Cz-DMAC-TXO and 2Cz-DMAC-TTR TADF exhibited voltage-independent EL emissions with peaks at 548, 572 and 608 nm and Commission Internationale del'Eclairage (CIE) coordinates of (0.39, 0.54), (0.47, 0.51) and (0.56, 0.42), respectively. Compared with their PL spectra in dilute toluene solution, the EL spectra of three compounds are obviously red-shifted, which should be mainly caused by the strong concentration aggregation in the film states. Meanwhile, the maximum current efficiencies, power efficiencies and EQEs of the OLEDs based on 2Cz-DMAC-BTB, 2Cz-DMAC-TXO and 2Cz-DMAC-TTR were 42.5, 18.3 and 4.9 cd/A, 37.1, 17.4 and 4.3 lm/W and 14.0%, 6.6% and 2.9%, respectively. As listed in Table S4 (Supporting information), the performance of 2Cz-DMAC-BTB is quite remarkable among the reported solution-processed non-doped TADF OLEDs, demonstrating the potential of 2Cz-DMAC segment to construct efficient solution-processable non-doped TADF emitters.

In this work, we developed a new electron-donating segment 2Cz-DMAC, which could simultaneously enhance the solubility and suppress harmful ACQ process. Based on 2Cz-DMAC, three new compounds were constructed as the solution-processable non-doped TADF emitters. As anticipated, 2Cz-DMAC-BTB, 2Cz-DMAC-TXO and 2Cz-DMAC-TTR exhibited obvious TADF behaviors with extremely small ΔE_{ST}s of 0.020, 0.036 and 0.047 eV as well as favorable solubility, thermal stability and film-forming ability. In the solution-processed neat films, 2Cz-DMAC-BTB, 2Cz-DMAC-TXO and 2Cz-DMAC-TTR exhibited high Φ_{PL}s of 68.0%, 32.2% and 12.6% and k_{RISC}s of 12.6 × 10^5, 8.6 × 10^5 and 5.7 × 10^5 s^{-1}, respectively. By employing 2Cz-DMAC-BTB, 2Cz-DMAC-TXO and 2Cz-DMAC-TTR as EMLs, the solution-processed non-doped OLEDs were optimized to exhibit green, orange and red EL emission with maximum EQEs of 14.0%, 6.6% and 2.9%, respectively. These results successfully confirm the feasibility and convenience of developing efficient solution-processable non-doped TADF emitters based on 2Cz-DMAC segment.

Declaration of competing interest

The authors declare that they have no known competing financial interests or personal relationships that could have appeared to influence the work reported in this paper.

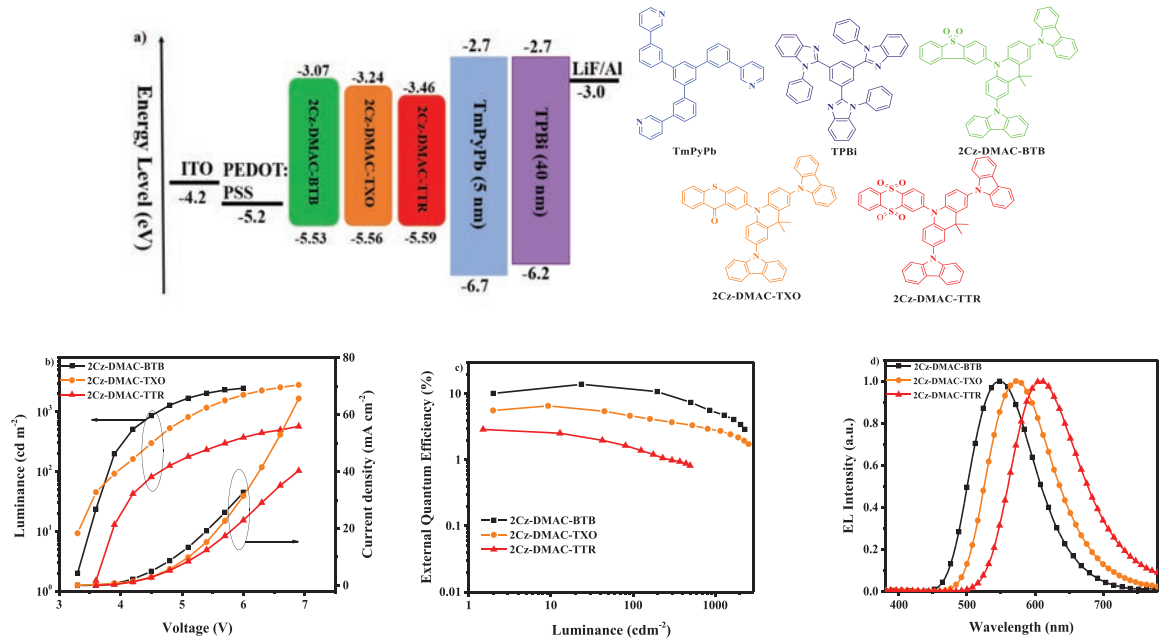

Fig. 4. (a) Energy level diagrams, (b) luminance-voltage-current density, (c) PE-EQE-luminance characteristics, (d) EL spectra of solution-processed OLEDs based on 2Cz-DMAC-BTB, 2Cz-DMAC-TXO and 2Cz-DMAC-TTR.

Acknowledgment

This work was supported by the National Natural Science Foundation of China (Nos. 51773029, 52073040 and 51821002), the Fundamental Research Funds for the Central Universities (No. ZYGX2016Z010) and the International Cooperation and Exchange Project of Science and Technology Department of Sichuan Province (No. 2019YFH0057).

Supplementary materials

Supplementary material associated with this article can be found, in the online version, at doi:10.1016/j.cclet.2021.08.064.

References

[1] H. Uoyama, K. Goushi, K. Shizu, H. Nomura, C. Adachi, Nature 492 (2012) 234–238.
[2] S. Hirata, Y. Sakai, K. Masui, et al., Nat. Mater. 14 (2015) 330–336.
[3] J.W. Sun, J.H. Lee, C.K. Moon, et al., Adv. Mater. 26 (2014) 5684–5688.
[4] D.R. Lee, B.S. Kim, C.W. Lee, et al., ACS Appl. Mater. Interfaces 7 (2015) 9625–9629.
[5] T.A. Lin, T. Chatterjee, W.L. Tsai, et al., Adv. Mater. 28 (2016) 6976–6983.
[6] L.W. T, M.J. Huang, C.C. Lin, et al., Nat. Photonics. 12 (2018) 235–240.
[7] W.X. Zeng, H.Y. Lai, W.K. Lee, et al., Adv. Mater. 30 (2018) 1704961.
[8] Y.L. Zhang, Q. Ran, Q. Wang, et al., Adv. Mater. 31 (2019) 1902368.
[9] X. Tang, L.S. Cui, H.C. Li, et al., Nat. Mater. 19 (2020) 1332–1338.
[10] H.G. Kim, K.H. Kim, J.J. Kim, Adv. Mater. 29 (2017) 1702159.
[11] D.D. Zhang, X.Z. Song, M.H. Cai, L. Duan, Adv. Mater. 30 (2018) 1705250.
[12] Z.H. Ma, W.Y. Dong, J.H. Hou, et al., J. Mater. Chem. C 7 (2019) 11845–11850.
[13] W. Li, B. Li, X.Y. Cai, et al., Angew. Chem. Int. Ed. 58 (2019) 11301–11305.
[14] Y.Z. Shi, K. Wang, X. Li, et al., Angew. Chem. Int. Ed. 57 (2018) 9480–9484.
[15] Y. Suzuki, Q.S. Zhang, C. Adachi, J. Mater. Chem. C (2015) 1700–1706.
[16] J. Huang, H. Nie, J.J. Zeng, et al., Angew. Chem. Int. Ed. 6 (2017) 12971–12976.
[17] J.J. Guo, X.L. Li, H. Nie, et al., Adv. Funct. Mater. 27 (2017) 1606458.
[18] L. Zhang, Y.F. Wang, M. Li, Q.Y. Gao, C.F. Chen, Chin. Chem. Lett. 32 (2021) 740–744.
[19] X. Li, K. Wang, Y.Z. Shi, et al., J. Mater. Chem. C 6 (2018) 9152–9157.
[20] Y.J. Cho, B.D. Chin, S.K. Jeon, J.Y. Lee, Adv. Funct. Mater. 25 (2015) 6786–6792.
[21] D. Liu, W.W. Tian, Y.L. Feng, et al., ACS Appl. Mater. Interfaces 11 (2019) 16737–16748.
[22] D.M. Sun, X.K. Zhou, H.H. Li, et al., ACS Appl. Mater. Interfaces 7 (2015) 17802–17810.
[23] K. Albrecht, K. Matsuoka, K. Fujita, K. Yamamoto, Angew. Chem. Int. Ed. 54 (2015) 5677–5682.
[24] Q. Li, J. Hu, J.H. Lv, et al., Angew. Chem. Int. Ed. 59 (2020) 20174–20182.
[25] Y.J. Cho, Y.J. Zhang, H. Yu, H. Aziz, Adv. Funct. Mater. 26 (2016) 8662–8669.
[26] K. Matsuoka, K. Albrecht, A. Nakayama, K. Yamamoto, K. Fujita, ACS Appl. Mater. Interfaces 10 (2018) 33343–33352.
[27] K. Albrecht, K. Matsuoka, K. Fujita, K. Yamamoto, Mater. Chem. Front. 2 (2018) 1097–1103.
[28] M. Godumala, S. Choi, H.J. Kim, et al., J. Mater. Chem. C 6 (2018) 1160–1170.
[29] L. Hua, S.K. Yan, Z.J. Ren, Acta. Polym. Sin. 51 (2020) 457–461.
[30] Z. Zhao, B. He, H. Nie, et al., Chem. Commun. 50 (2014) 1131–1133.
[31] G. Kreiza, B. Banevičius, J. Jovaišaitė, et al., J. Mater. Chem. C 7 (2019) 11522–11531.
[32] X.L. Chen, J.H. Jia, R.M. Yu, et al., Angew. Chem. Int. Ed. 56 (2017) 15006–15009.
[33] Y.H. Kim, C. Wolf, H. Cho, S.H. Jeong, T.W. Lee, Adv. Mater. 28 (2016) 734–741.
[34] Y. Xiong, J. Zeng, B. Chen, et al., Chin. Chem. Lett. 30 (2019) 592–596.
[35] H. Xu, Z.F. Xu, Z.Y. Yue, et al., J. Phys. Chem. C. 112 (2008) 15517–15525.
[36] X.X. Ban, A.Y. Zhu, T.L. Zhang, et al., ACS Appl. Mater. Interfaces 9 (2017) 21900–21908.
[37] J. Lee, N. Aizawa, M. Numata, C. Adachi, T. Yasuda, Adv. Mater. 29 (2017) 1604856.
[38] J.J. Luo, S.L. Gong, Y. Gu, et al., J. Mater. Chem. C 4 (2016) 2442–2446.
[39] M.L. Huang, Y.F. Li, K.L. Wu, et al., Dyes. Pigm. 153 (2018) 92–98.
[40] Y.F. Li, T.H. Chen, M.L. Huang, et al., J. Mater. Chem. C 5 (2017) 3480–3487.
[41] Z. Ma, Y. Wan, W. Dong, et al., Chin. Chem. Lett. 32 (2021) 703–707.
[42] Y.F. Li, G.H. Xie, S.L. Gong, K.L. Wu, C.L. Yang, Chem. Sci. 7 (2016) 5441–5447.
[43] S.Y. Park, S. Choi, G.E. Park, et al., ACS Appl. Mater. Interfaces 10 (2018) 14966–14977.
[44] Y. Liu, X. Wei, Z. Li, et al., ACS Appl. Energ. Mater. 1 (2018) 543–551.
[45] S. Wang, Z. Cheng, X. Song, et al., ACS Appl. Mater. Interfaces 9 (2017) 9892–9901.
[46] J.X. Chen, K. Wang, C.J. Zheng, et al., Adv. Sci. 5 (2018) 1800436.
[47] Q. Zhang, H. Kuwabara, W.J. Potscavage, et al., J. Am. Chem. Soc. 136 (2014) 18070–18081.